Title:

Fluidization of high-density particles: The influence of fines on reactor performance

Author names and Affiliations:

Jean Saayman[1], Naoko Ellis[2] and Willie Nicol[1]*

[1] *Department of Chemical Engineering*

University of Pretoria - Main Campus

Corner Lynwood Rd & Roper St

Hatfield

Pretoria

0002

South Africa

[2] *Department of Chemical and Biological Engineering*

University of British Columbia

2360 East Mall

Vancouver, BC

Canada

V6T 1Z3

* *Corresponding author*: ***Willie Nicol***

Email:	*willie.nicol@up.ac.za*
Tel:	*+2712 420 3796*
Fax:	*+2712 420 5048*
Postal Address:	*Willie Nicol*
	University of Pretoria
	Department of Chemical Engineering
	Pretoria
	South Africa
	0002

REACTOR PERFORMANCE

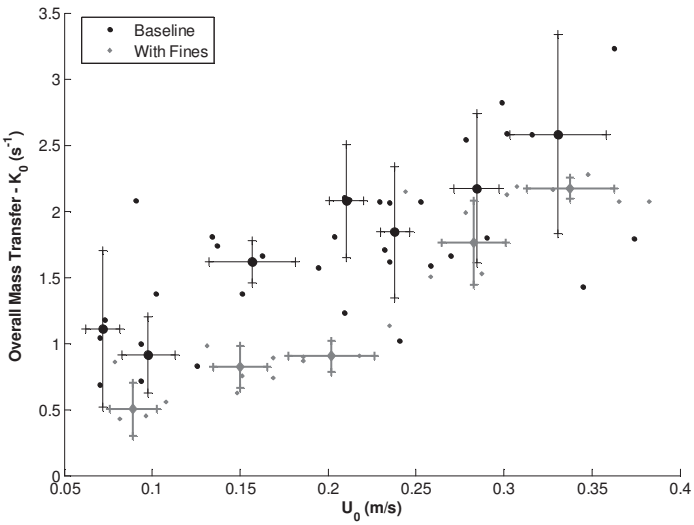

VOIDAGE DISTRIBUTION

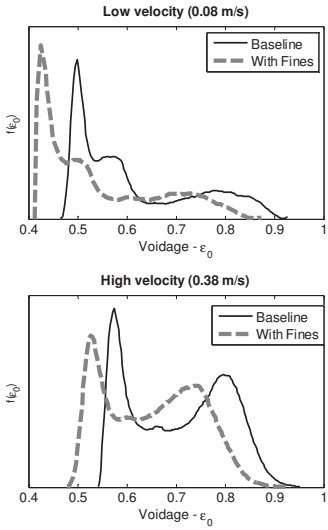

Abstract

The effect of fines on the hydrodynamics of a gas-solid fluidized bed and ozone decomposition reaction was investigated using high-density iron-silicon (FeSi) particles with a particle density of 6690 kg/m^3. The addition of fines decreased the bubble size, dense phase voidage and reactor performance. The bubble size decrease is in accordance with reported literature; while, increase in dense phase voidage and reactor performance were found in the literature on less dense catalyst. The reactor performance was quantified using an apparent overall mass transfer parameter derived from fitting a two-phase model to the experimental data. The method allowed for reactor performance comparison despite the fluctuation in FeSi particle activity. Model fitting results suggest that smaller bubbles should improve mass transfer in addition to reactor performance. However, the decreased dense phase voidage with addition of fines counteracted the effects of smaller bubbles. Higher entrainment rate of the bed with fines were noted.

KEYWORDS: Reactor performance, High-density particles, Fines, Voidage distributions, Ozone decomposition reaction

1 Introduction

Gas-solid fluidized beds are widely used in chemical and petrochemical industries owing to their efficient contact between the phases, resulting in good mixing and superior heat and mass transfer. Although the open literature contains numerous studies on fluidized bed hydrodynamics, very little is reported on highly dense particles [1,2]. The High-Temperature Fisher-Tropsch (HTFT) gas-solid fluidized bed is a unique example of an industrial process employing high-density particles with an estimated particle density ranging from 7,000 to 9,000 kg/m^3 [3,4].

The addition of fines in gas-solid fluidized beds has long been known to introduce desirable features into reactors. In industry, fines are mostly generated via attrition during normal reactor operation. For bubbling fluidized beds, a decrease in bubble size and an increase in dense phase voidage have been reported. This is in agreement with a longer collapse time for fluidized beds containing higher fines [5–8]. The mechanisms by which the addition of fines influences the hydrodynamics are still unclear. Some research suggests that in gas-solid fluidized beds the particles tend to form stable agglomerates when they are smaller than 20–40 μm [9]. From SEM images it was found that fine particles adhered to coarse particles or formed agglomerates [10]. Other effects of fines include the decrease of the velocity at which the turbulent fluidization regime starts [11–13]. Furthermore, the effect of fines on elutriation from fluidized beds was found to depend on the size and proportion of fines, as well as the gas velocity [9]. A more recent and systematic study has shown the influence of particle size distribution and the addition of fines on the hydrodynamic behaviour of Geldart A particles [14].

The change in hydrodynamics with addition of fines has also been proved to increase conversion in a catalytic reaction system. Yates and Newton [15] added 16% and 27% fines to a bed of Geldart A commercial oxidation catalyst, where fines were defined as particles <45 μm. The investigation found that reactor performance increased due to an increase in dense phase voidage. The voidage increase caused a shift in the gas flow pattern: more gas was flowing through the dense phase and less in the lean phase. Further experimental evidence was reported by Sun and Grace [16] on the disproportionate increase of fines contained in bubbles contributing to better chemical conversion with a wider particle size distribution [11]. The study was conducted with a narrow, bimodal and wide particle size distribution of Fluid Catalytic Cracking (FCC) catalyst. Fines were defined as particles smaller than 20% of the Sauter mean particle size.

The aim of this investigation was to observe the effect of fines on the reactor performance of dense particle fluidization. The velocity range included the bubbling and turbulent fluidization flow regimes, since the turbulent regime is generally associated with less interphase mass transfer restriction and, accordingly, improved reactor performance. Initial work on the technique of quantifying reactor performance was done using an FCC catalyst in a pseudo 2D column [17,18]. For this investigation the technique was refined and a different reactor modelling approach was used to gain insight into changes in reactor performance. High-density iron-silicon (FeSi) alloy particles were then used in a 3D cold bed. Conversion was determined using the ozone decomposition reaction,

which is catalysed by naturally active FeSi particles. Additional hydrodynamic measurements included bubble size, solids concentration and entrainment rate.

2 Experimental approach

2.1 Basic two-phase reactor model

As with most multiphase reactors, modelling of a fluidized bed is complex due to hydrodynamic behaviour. Two-phase theory is now generally accepted as the best modelling approach [19–21]. At its simplest, a fluidized bed reactor can be described as a dense solids-rich phase with a lean solids-deprived phase bubbling through it. Reactant, mostly in the lean phase, is transported to the dense phase via mass transfer in which most of the reaction occurs. By assuming negligible gas flow through the dense phase and no solids content in the bubbling phase, the following mass balance can be done based on the solids volume of the catalyst:

$$C_i = u_b C_{i,B} + u_E C_{i,E} \tag{1}$$

$$A_{bed} u_b \frac{dC_{i,B}}{dV_s} = -K_O (C_{i,B} - C_{i,E}) \tag{2}$$

$$A_{bed} u_E \frac{dC_{i,E}}{dV_s} = -R_i(\boldsymbol{C_E}) + K_O (C_{i,B} - C_{i,E}) \tag{3}$$

where R_i is the reaction rate. For first order reactions it would be:

$$R_i(\boldsymbol{C}) = k_r \tag{4}$$

In this model the overall mass transfer coefficient (K_0) has the same units as k_r, which is based on the rate of total volumetric gas transfer per solids volume. It is important to understand that if K_0 is fitted to experimental data using this simple two phase model; it would be an apparent parameter; the concept is similar to an apparent reaction rate constant. When a reaction rate constant (k_R) is determined by fitting a Plug Flow Reactor (PFR) model to packed bed experimental data, flow effects or hydrodynamics would be incorporated in the value of k_R. The value of K_0 will be influenced by hydrodynamic behaviour which is not considered in the model. This apparent overall coefficient serves as an indicator of the reactor performance, irrespective of the catalytic activity of the bed. K_0 should not be seen as the actual mass transfer in the bed, but rather the measurement of reactor performance.

By taking into account the hydrodynamics of the reactor and the K_0 parameter, the generally used area-specific mass transfer coefficient can be calculated. K_0 should be multiplied by the ratio of solids to expanded bed and divided by the bubble fraction and the ratio of bubble volume to surface area:

$$k_{be} = \frac{K_O (\frac{V_p}{V_{bed}})}{\psi_B \, a_i} \tag{5}$$

where

$$\frac{V_p}{V_{bed}} = (1 - \varepsilon_0) \tag{6}$$

$$\psi_B = \frac{u_0}{u_{br}} \text{ [22]} \quad (7)$$

For the bubble rise velocity (u_{br}):

$$u_{br} = 0.711\sqrt{gD_b} \quad (8)$$

From this discussion it is clear that k_{be}, is dependent on correlations, assumptions and model selection. A popular area-specific mass transfer correlation is that of Sit and Grace [23]:

$$k_{be} = \frac{1}{3}U_{mf} + \left(\frac{4D_m\varepsilon_{mf}U_{br}}{\pi D_b}\right)^{\frac{1}{2}} \quad (9)$$

2.2 Bubble measurement techniques

Two methods of bubble measurement were used in this investigation: an intrusive probe technique and a non-intrusive pressure measurement technique. The intrusive technique makes use of a voidage probe which detects a passing bubble due to a sudden drop in solids concentration around the probe. Using the probe-bubble contact time and a bubble rise velocity correlation, the bubble size is estimated. Karimipour and Pugsley [24] did a critical evaluation of all the available correlations, from which the most appropriate correlation was chosen for this system. The correlation of Werther (1978, included by the above authors) was used by taking the average between the Geldart A and B correlations; FeSi is at the boundary between A and B:

$$u_{br} = 0.934\sqrt{9.81D_b} \quad (10)$$

It is important to note that there is a difference between the average bubble size and the void length. To relate the void length distribution to an average bubble size, the equation of Liu and Clark [25] is required:

$$L_b = \left(\frac{2}{3}\alpha(1+Q)^3 - \alpha Q(1+Q)^2\right)D_b \quad (11)$$

where Q is the bubble wake shape factor.

With the probe-bubble contact time (t_1) and rise velocity correlation, a void length can now be determined:

$$L_b = t_1 u_{br} \quad (12)$$

and it can be shown that:

$$D_b = \frac{8.56}{\left(\frac{2}{3}\alpha(1+Q)^3 - \alpha Q(1+Q)^2\right)^2}t_1^2 \quad (13)$$

The non-intrusive technique of Beetstra et. al. [14], which uses pressure measurement signals, was also used. The Power Spectral Density (PSD) function of the signals is used to decompose pressure fluctuations into global bed phenomena and phenomena in the vicinity of the pressure probe. These local phenomena are caused by the passing bubbles/voids. Two pressure probes are required: one in

the plenum chamber or directly above the distributor, and a second at a height in the bed where bubble measurement is desired. The PSDs of both pressure probe signals are compared and the incoherence of the two signals relative to each other is calculated. The standard deviation of this incoherence (σ_i) is a measure of the average bubble/void size. This is directly proportional to the bubble size in the following manner:

$$D_b \propto \frac{\sigma_i}{\rho_b g} \tag{14}$$

which means:

$$D_b \propto \frac{\sigma_i}{\rho_p(1-\varepsilon_0)g} \tag{15}$$

2.3 Equipment and method

The investigation was conducted using a 0.14 m inside diameter acrylic column of height 5.5 m. To return entrained solids to the bed, a system with two external cyclone returns was used. Filter bags were installed after the cyclones and weighed before and after experiments. A triangular pitch perforated plate distributor with thirty 2 mm holes was used with an open area of 0.61%. To prevent solids weepage, a porous cloth was placed below the distributor. The particles used for these experiments were a high-density FeSi alloy – ±86 wt.% iron and ±14 wt.% silicon, with the particle properties listed in Table 1.

Vortex flow meters were used for fluidizing gas velocities in the range of 0.06 to 0.45 m/s. A rotameter was employed for velocities below this range. Three absolute pressure probes were installed in the bed at 0, 0.20 and 0.40 m above the distributor plate. A reflective-type optical probe, for voidage measurements, was inserted at 0.2 m from the distributor. The voidage probe was calibrated by submerging it in non-fluidized catalyst (dense phase reading) and in a dark solids-free tube. A linear calibration was assumed between these two points.

The ozone decomposition reaction was used as the tracer reaction to quantify reactor performance. Ozone was discharged via a stack; an exhaust system with a solids-filter-bag container was installed after the cyclones to remove any remaining solids safely before ozone-containing air was sent to the stack. To determine catalyst activity, a small test reactor with plug flow behaviour, 16.4 mm in diameter, was installed. Both the fluidized bed reactor (FBR) and the test reactor were supplied with the same ozone-dosed air. The test reactor could be loaded by tapping catalyst directly from the fluidized bed into it, thereby not exposing the sample to an atmosphere other than that inside the FBR. Figure 1 schematically shows the equipment setup.
Insert Figure 1

Ozone decomposes to oxygen with a heat of reaction (ΔH_{298}) of -138 kJ/mol and a free energy of reaction (ΔG_{298}) of -163 kJ/mol, but it is thermally stable up to 523 K [18]. Metals and metal oxides serve as good catalysts [26] although metal oxides are preferred. Most of these catalysts have varying deactivation trends which are influenced by factors such as the presence of NO_x, humidity and oxygen, but all researchers have found that first-order kinetics apply [17,26–28]. This reaction is ideally suited for investigations in a fluidized bed as it is first order and can be conducted at ambient

temperature and low concentrations, which result in negligible volume change. FeSi, which is 84–86% iron, is naturally active for ozone decomposition.

The fluidizing medium was air supplied by a compressor with a chiller maintaining the air at a constant temperature of 15 °C. The air was dosed with ozone generated with the EcoTec MZV1000 cold corona ozone generator, using oxygen as feed gas to ensure that no NO_x gases form. To ensure proper gas mixing, a freely rotating turbine rotor was installed after the dosing point. The plenum chamber was also filled with 6 mm diameter glass beads. A gas sampling tube, for determining the inlet ozone concentrations, was inserted into the centre of the plenum chamber, 50 mm below the distributor. Outlet samples were drawn from the centre of the reactor, 4.2 m above the distributor. The ozone sampling probes were covered with filter paper to prevent solids from entering the analyser. The samples were continuously analysed online using the 2B Technology Inc. UV-106 ozone analyser, which employs the well-established method of light adsorption at a wavelength of 254 nm. All data were logged using 4–20 mA or 0–10V signals in conjunction with National Instruments' USB-6008 DAQ devices connected to a PC. Flow meter and ozone concentrations were logged at 10 Hz and the voidage probe measurements were collected at 1,000 Hz for 10–15 min.

A total of 37 kg of FeSi was loaded into the reactor, resulting in a packed bed height of 0.57 m after steady-state operation. Using the bulk density, it was determined that 13.5% of the catalyst was in the return system. For the range of superficial gas velocities studied (0.062 m/s < U < 0.389 m/s), the settled bed height was in the range of 0.565–0.575 m, i.e., a 0.9% fluctuation, which was deemed negligible. First-order behaviour of the catalyst was confirmed by taking approximately 30 g of catalyst and loading it into the test reactor. Conversion was determined at different flow rates and inlet concentrations. A first order reaction rate model predicted these conversion results accurately. The FBR and test reactor were run in parallel in order to obtain the catalyst activity for each conversion reading taken for the FBR. It was confirmed that the inlet concentrations for both test reactor and FBR were the same. The test reactor was operated at a single velocity since first-order behaviour was known. After each FBR outlet reading, a catalyst sample was taken and the activity determined within 5 minutes. In this manner a pseudo-instantaneous catalyst activity was obtained. By taking a sample of the bed and testing the catalytic activity for each measurement of the reactor's conversion, variations in the bed activity are accounted for. The superficial gas velocity in the FBR was changed randomly to prevent possible hysteresis effects. Fines were added by removing 10 kg (27 wt.% of the bed) of the baseline mixture and replacing it with 10 kg of fines having a mean diameter of 21 µm. Figure 2 shows the PSDs, before and after fines were added.As can be seen in Table 1, the minimum fluidization, determined experimentally, decreased from 6.5 to 5.0 mm/s. Other system properties are also reported in the table.
Insert Figure 2
Insert Table 1

3 Results and Discussion

Bubble sizes, voidage probe data, absolute pressure readings, overall reactor conversion and pseudo-instantaneous catalyst activity (first-order rate constant) were logged. Voidage probe data for the baseline were not available for all the data sets. Using the basic two-phase model, reactor conversion and catalyst activity, the apparent overall mass transfer coefficient (K_0) could be

determined. This was achieved by fitting the model conversion to the actual conversion, with an error smaller than ±3%.

3.1 Reactor performance

In our previous work, the Thompson et al. [20] model was used to do a best fit of the reactor performance efficiency over the velocity range and from that ascertain the mass transfer and axial dispersion [17,18]. As show by both Brink et. al. [17] and Saayman [20], the shape of the fitted curve is dependent on the catalyst activity; therefore, if the activity changes significantly, the method fails. Catalyst activity for FeSi fluctuates between 0.5 and 4.5 s^{-1}, constituting a major variation. This is shown in Figure 3a, the catalyst activity is plotted for each run's measurement. Due to the variation in the bed's activity, considerable scatter is seen in the conversion data for a certain velocity (Figure 3b).
Insert Figure 3

An alternative interpretation had to be used in which data points could be evaluated individually, hence the use of the apparent overall mass transfer (K_0). The advantages are that only one parameter is fitted, and all complexities of the Thompson et al. [20] model are avoided. The apparent overall mass transfer calculated from the experimental results is plotted in Figure 4, showing an increasing trend with superficial velocity. It is well known that fluidized beds perform better at higher velocities, especially in the turbulent fluidization flow regime which has vigorous gas-solid contacting [29]. With the addition of fines, bubble sizes generally decrease and a better quality of fluidization is achieved. We visually noted that the bubbles were smoother and better defined. As previous researchers have found [15,30], it would be expected that better reactor performance is achieved. However, Figure 4 does not show any advantages from adding fines to the system. Overall, the reactor performed worse, except at higher superficial velocities where the statistically observable difference disappears. An in-depth investigation of the hydrodynamic differences between these two systems was performed to address why this unexpected behaviour was observed.
Insert Figure 4

3.2 Hydrodynamics

The transition between the bubbling and turbulent fluidization flow regimes was determined using the standard deviation of pressure fluctuations technique [29]. Using absolute pressure measurement a clear trend in the standard deviation could not be found. However, the differential pressure measurements between the 20 and 40 cm probes did show a clear trend, as seen in Figure 5. The absolute pressure fluctuations could have been influenced by some unknown phenomenon in the plenum chamber or more likely in the exhaust system. From the results of the analysis, u_c is at 0.36 m/s for the baseline system and at 0.33 m/s for the case with added fines, which are much lower than those suggested by the correlations, i.e., in the order of 0.7 to 0.9 m/s. It should, however, be noted that the highest particle density used to obtain these correlations is 2,970 kg/m^3.[31] Turbulent regime was confirmed from visual observations; features such as the diffused expanded bed surface and chaotic void movement were observed. Transition to the

turbulent flow regime explains why the difference in reactor performance of the two particle mixtures disappears at the higher velocities.

Insert Figure 5

Figure 6 shows the results of the bubble size derived from the voidage probe. The bubble size correlation of Cia et al. (1994, taken from Karimipour and Pugsley,2011) [24]is used in conjunction with a fitting parameter to obtain an equation for the bubble size:

$$D_{b-Correlation} = 0.138h^{0.8}(u_0 - u_{mf})^{0.42}e^{\left\{-2.5\times10^{-5}(u_0-u_{mf})^2 - 10^{-5}(u_0-u_{mf})\right\}} \quad (16)$$

$$D_{b-FIT} = k_{db} * D_{b-Correlation} \quad (17)$$

$$D_{b-FIT} = k_{db} * 0.138h^{0.8}(u_0 - u_{mf})^{0.42}e^{\left\{-2.5\times10^{-5}(u_0-u_{mf})^2 - 10^{-5}(u_0-u_{mf})\right\}} \quad (18)$$

k_{db} is 2.92 and 1.90 for the baseline case and the added fines case, respectively. Figure 7 is the incoherent standard deviation divided by $\rho_p(1-\varepsilon_0).g$. The trends between these readings are fairly similar. As found by Beetstra et al. [14], bubble sizes decrease with the addition of fines, which is evident in both Figures 6 and 7. As the superficial velocity is increased, the effect is enhanced even further. It is also noted that the bubble size is less sensitive to gas velocity when fines are added. This observed behaviour is characteristic of Geldart A particles. The baseline particles are already close to border between Geldart A and B particles, while the addition of fines shifts the classification closer to Geldart A particles."

Insert Figure 6

Insert Figure 7

The mean voidage was calculated by averaging 5 minutes of voidage probe data at a specific velocity. Data are not available for all the runs of the baseline case. Figure 8 shows the results; the case with added fines clearly has a lower overall bed voidage, suggesting lower bubble or gas holdup.

Insert Figure 8

Figure 9 shows the voidage distributions of the baseline case and the case with added fines, at a low flow rate (0.08 m/s) and a high flow rate (0.38 m/s). For both cases two-phase behaviour is observed, which is evident from the bimodal distributions. The mean voidage value of the position of each peak is shown. The dense phase (sharp peak at low voidage) has a higher value for the baseline case at both sets of velocities, suggesting that the dense part of the bed would be more expanded for the baseline case. The irregular shape of this peak is probably caused by the intrusive nature of the probe. The peak representing bubble voidage (second peak at higher voidage) has a higher value for the baseline case, meaning less solids content in the bubble.

At the higher velocity, the two-phase structure is starting to break down for the case when fines are added. The dense bed voidage and bubble voidage are much closer to each other and the dip between the two peaks is not as prominent. An even solids distribution spread would explain why the reactor performance increases at higher velocities. Previous researchers found voidage increases with the addition of fines, whereas Figures 8 and 9 show the opposite when using FeSi [14,15]. The considerable difference in particle densities may play a role in these discrepancies.

Insert Figure 9

3.3 Specific mass transfer

To tie the hydrodynamic measurements in with reactor performance, the overall mass transfer (K_0) was recalculated while taking into account conversion in the freeboard. This newly determined K_0 was then converted to the specific mass transfer (k_{be}). The freeboard model of Kunii and Levenspiel [32] was used. In this model the entrainment is required to determine the solids concentration profile in the freeboard:

$$1 - \varepsilon_{top} = \frac{G_s}{\rho_s(u_0 - u_t)} \tag{19}$$

Entrainment rate (G_s) measurements are reported in Figure 10. Each data point is based on three repeat runs. Entrainment is higher when fines are added to the bed, although the difference in entrainment between the "baseline" and "with fines" cases did not affect the relative results of specific mass transfer (k_{be}). The resulting k_{be} curve in Figure 11 shows a similar trend in the data and correlation. The measured bubble sizes were used to calculate the value of the correlation for k_{be}. Qualitatively, the correlation seems to work as it predicts mass transfer for the baseline case with reasonable accuracy. For the added fines case, the correlation considerably overpredicts mass transfer. Most researchers need to apply some correction factor to correlations, which was not done for this case [17,20,33].

Insert Figure 10

Insert Figure 11

The method used to obtain Figure 11 is very dependent on the assumptions of the reactor model. Firstly, it is assumed that the bubbles are free of solids, which is not the case. Secondly, it is assumed that all flow goes through the bubble phase, but one of the hydrodynamic factors not considered is through-flow in the dense phase. Both of these factors will influence the absolute values of k_{be}.

From Figure 9 an explanation can be postulated as to why the bed without fines performs better. The dense phase is more expanded for the baseline case, meaning higher gas holdup and more gas flow in the dense phase where most of the reaction takes place. As mentioned, fines tend to form agglomerates, which is a possible mechanism by which the addition of fines improves reactor performance. It is speculated that the increased particle density effectively prevents agglomerates from forming, which would explain the unexpected results. Further investigation into this aspect of high-density particle fluidization is required.

4 Conclusions

With high-density FeSi particles the study has shown that the addition of fines decreased the overall reactor performance. Dense phase voidage unexpectedly decreased with the addition of fines, decreasing the through-flow in the dense phase and providing a likely explanation for the decrease in reactor performance. This behaviour is contrary to previous studies where bed voidage increased. The effect of fines on the bubble sizes and the bubbling-turbulent transition velocity decreased, in line with other studies. However, these changes did not improve the reactor performance, which

suggests that the decrease in dense phase voidage seemed to have a greater effect on performance. Entrainment rates increased with the addition of fines. Specific mass transfer coefficient was calculated based on reactor modelling assumptions and the baseline case agrees well with the Sit and Grace correlation [23].

Nomenclature

A_{bed}	Cross-sectional area of bed	[m^2]
a_i	Bubble surface area per bubble volume (=6/D_b)	[m^{-1}]
C_B	Concentration in bubble	[mol/m^3]
C_E	Concentration in emulsion	[mol/m^3]
C_i	Gas concentration of species I	[$kmol/m^3$]
D_b	Bubble diameter	[m]
D_m	Gas diffusion coefficient	[m^2/s]
d_p	Particle diameter	[m]
g	Gravitational acceleration (9.81)	[m/s^2]
G_s	Solids circulation rate/entrainment rate	[$kg/s.m^2$]
h	Height above distributor	[m]
k_{be}	Specific bubble-emulsion mass transfer coefficient	[m/s]
K_O	Apparent bubble-emulsion mass transfer coefficient (based on catalyst volume)	[s^{-1}]
k_r	Reaction rate constant (based on catalyst volume)	[s^{-1}]
Q	Ellipsoidal bubble wake shape factor	[-]
S_b	Surface area of bubble	[m^2]
t_1	Probe-bubble contact times	[s]
u_b	Bubble velocity	[m/s]
u_{br}	Single bubble rise velocity	[m/s]
u_E	Emulsion phase velocity	[m/s]
u_{mf}	Minimum fluidization velocity	[m/s]
u_o	Operating velocity	[m/s]
u_t	Terminal particle velocity	[m/s]
V_{bed}	Total volume of reactor bed	[m^3]
V_p	Total volume of solids particles	[m^3]

Subscripts

B	Bubble phase (low density phase)
b	Bubble
E	Emulsion phase (high density phase)
mf	Minimum fluidization
top	Top of freeboard

Greek letters

α	Ellipsoidal bubble shape factor	[-]
ε	Gas volume fraction	[-]
ε_0	Porosity of fluidized bed at operating velocity	[-]

ρ_b	Bulk density	[kg/m^3]
ρ_p	Particle density	[kg/m^3]
ρ_g	Gas density	[kg/m^3]
σ_i	Standard deviation of incoherence	[Pa]
μ_g	Gas viscosity	[Pa.s]
ψ	Phase volume fraction	[-]

References

[1] A. Bischi, Ø. Langørgen, J.-X. Morin, J. Bakken, M. Ghorbaniyan, M. Bysveen, et al., Performance analysis of the cold flow model of a second generation chemical looping combustion reactor system, Ener. Proc. 4 (2011) 449–456.

[2] W. de Vos, W. Nicol, E. du Toit, Entrainment behaviour of high-density Geldart A powders with different shapes, Powder Technol. 190 (2009) 297–303.

[3] D.J. Duvenhage, T. Shingles, Synthol reactor technology development, Catal. Today. 71 (2002) 301–305.

[4] A. P. Steynberg, R.L. Espinoza, B. Jager, A. C. Vosloo, High-temperature Fischer–Tropsch synthesis in commercial practice, App. Catal. A: Gen. 186 (1999) 41–54.

[5] H.O. Kono, C.C. Huang, E. Morimoto, T. Nakayama, T. Hikosaka, Segregation and agglomeration of Type C powders from homogeneously aerated Type A–C powder mixtures during fluidization, Powder Technol. 53 (1987) 163–168.

[6] P.U. Foscolo, R. Di Felice, L.G. Gibilaro, An experimental study of the expansion characteristics of gas fluidized beds of fine catalysts, Chem. Eng. Process. 22 (1987) 69–78.

[7] , J. Coca, Fines effects on collapsing fluidized beds, Powder Technol. 131 (2003) 234–240.

[8] R.J. Dry, I.N. Christensen, G.C. Thomas, The effect of naturally-occurring interparticle forces on the fluidization characteristics of fine iron oxide powders, Chem. Eng. Sci. 43 (1988) 1033–1038.

[9] J. Baeyens, S. Geldart, S.Y. Wu, Elutriation of fines from gas fluidized beds of Geldart A-type powders–effect of adding superfines, Powder Technol. 71 (1992) 71–80.

[10] X. Ma, K. Kato, Effect of interparticle adhesion forces on elutriation of fine powders from a fluidized bed of a binary particle mixture, Powder Technol. 95 (1998) 93–101.

[11] J.R. Grace, G. Sun, Influence of particle size distribution on the performance of fluidized bed reactors, The Canadian Journal of Chemical Engineering. 69 (1991) 1126–1134.

[12] D. Bai, Y. Masuda, N. Nakagawa, K. Kato, Transition to turbulent fluidization in a binary solids fluidized bed, Can. J. Chem. Eng. 74 (1996) 58–62.

[13] J.-H. Choi, H.-J. Ryu, C.-K. Yi, Type transition in onset condition of turbulent fluidization, Korean J. Chem. Eng. 28 (2011) 2009–2011.

[14] R. Beetstra, J. Nijenhuis, N. Ellis, J.R. van Ommen, The Influence of the particle size distribution on fluidized bed hydrodynamics using high-throughput experimentation, AIChE J. 55 (2009) 2013–2023.

[15] J.G. Yates, D. Newton, Fine particle effects in a fluidized-bed reactor, Chem. Eng. Sci. 41 (1986) 801–806.

[16] G. Sun, J.R. Grace, The effect of particle size distribution on the performance of a catalytic fluidized bed reactor, Chem. Eng. Sci. 45 (1990) 2187–2194.

[17] H.G. Brink, J. Saayman, W. Nicol, Two-dimensional fluidised bed reactor: Performance of a novel multi-vortex distributor, Chem. Eng. J. 175 (2011) 484–493.
[18] J. Saayman, Bubbling to turbulent regime transition in a 2D catalytic fluidized bed reactor, MSc dissertation, University of Pretoria, 2009.
[19] R. Jafari, R. Sotudeh-Gharebagh, N. Mostoufi, Performance of the wide-ranging models for fluidized bed reactors, Adv. Powder Technol. 15 (2004) 533–548.
[20] M. Thompson, H. Bi, J.R. Grace, A generalized bubbling/turbulent fluidized-bed reactor model, Chem. Eng. Sci. 54 (1999) 3–10.
[21] I.A. Abba, J.R. Grace, H.T. Bi, Spanning the flow regimes : Generic fluidized-bed reactor model, AIChE J. 49 (2003) 1838–1848.
[22] D. Kunii, O. Levenspiel, Fluidization Engineering, 2nd ed., Butterworth-Heinemann, Boston, 1991.
[23] S.P. Sit, J.R. Grace, Effect of bubble interaction on interphase mass transfer in gas fluidized beds, Chem. Eng. Sci. 36 (1981) 327–335.
[24] S. Karimipour, T. Pugsley, A critical evaluation of literature correlations for predicting bubble size and velocity in gas–solid fluidized beds, Powder Technol. 205 (2011) 1–14.
[25] W. Liu, N.N. Clark, Relationships between distribution lengths and distributions of chord of bubble sizes including their statistical parameters, International Journal of Multiphase Flow. 21 (1995) 1073–1089.
[26] B. Dhandapani, S.T. Oyama, Gas phase ozone decomposition catalysts, App. Catal. B: Environ. 11 (1997) 129–166.
[27] W.T. Tsai, C.Y. Chang, F.H. Jung, C.Y. Chiu, W.H. Huang, Y.H. Yu, et al., Catalytic decomposition of ozone in the presence of water vapor, J. Environ. Sci. Health, Part A. 33 (1998) 1705–1717.
[28] C.Y. Chang, W.T. Tsai, L. Cheng, Catalytic decompostion of ozone in air, J. Environ. Sci. Health. Part A: Environ. Sci. Eng. Toxicol. 32 (1997) 1837–1847.
[29] H.T. Bi, N. Ellis, I.A. Abba, J.R. Grace, A state-of-the-art review of gas-solid turbulent fluidization, Chem. Eng. Sci. 55 (2000) 4789–4825.
[30] J.R. Grace, G. Sun, Fines concentration in voids in fluidized beds, Powder Technol. 62 (1990) 203–205.
[31] J. Arnaldos, J. Casal, Prediction of transition velocities and hydrodynamical regimes in fluidized beds, Powder Technol. 86 (1996) 285–298.
[32] D. Kunii, O. Levenspiel, The KL reactor model for circulating fluidized beds, Chem. Eng. Sci. 55 (2000) 4563–4570.
[33] W. Wu, P.K. Agarwal, The Effect of Bed Temperature on mass transfer fluidized bed, Can. J. Chem. Eng. 81 (2003) 940–948.

Captions

Figure captions

Figure 1: Experimental setup. Both reactors are fed with the same gas and the small test reactor can be loaded online with catalyst

Figure 2: Particle size distributions before and after the addition of fines

Figure 3: (a) The catalytic activity of the bed measured in the test PFR, shown in chronological order. (b) Measured conversion data for the superficial velocity range.

Figure 4: Overall mass transfer coefficient showing an increasing trend. Statistical analysis was applied to every 5 consecutive data points for the "baseline" case and every 4 consecutive data points for the "with fines" case. Bar plots indicate the relevant mean and standard deviations in the x- and y-direction of this analysis

Figure 5: Standard deviations of differential pressure fluctuations show an u_c of 0.36 m/s for the baseline and 0.33 m/s for the case of added fines

Figure 6: Bubble sizes from the voidage probe, showing equivalent void diameter at 0.20 m above the distributor

Figure 7: Incoherent standard deviation at 20 cm, divided by the bed bulk density and gravitational constant

Figure 8: Overall bed voidage showing lower bubble hold-up for fines. These readings are from the voidage probe at r/R=0.5 and h=0.20 m

Figure 9: The voidage distribution of a 60 s measurement at r/R = 0.5 and 0.2 m from the distributor. The lowest (0.08 m/s) and highest (0.38 m/s) superficial velocities for the baseline case and the case with added fines are shown

Figure 10: Entrainment measurements for the specific mass transfer calculations

Figure 11: Specific mass transfer with superficial velocity. A statistical analysis was applied to every 5 consecutive data points for the “baseline” case and every 4 consecutive data points for the “with fines” case. Bar plots indicate the relevant mean and standard deviations in the x- and y-direction of this analysis

Table 1: Catalyst and fluidizing medium properties

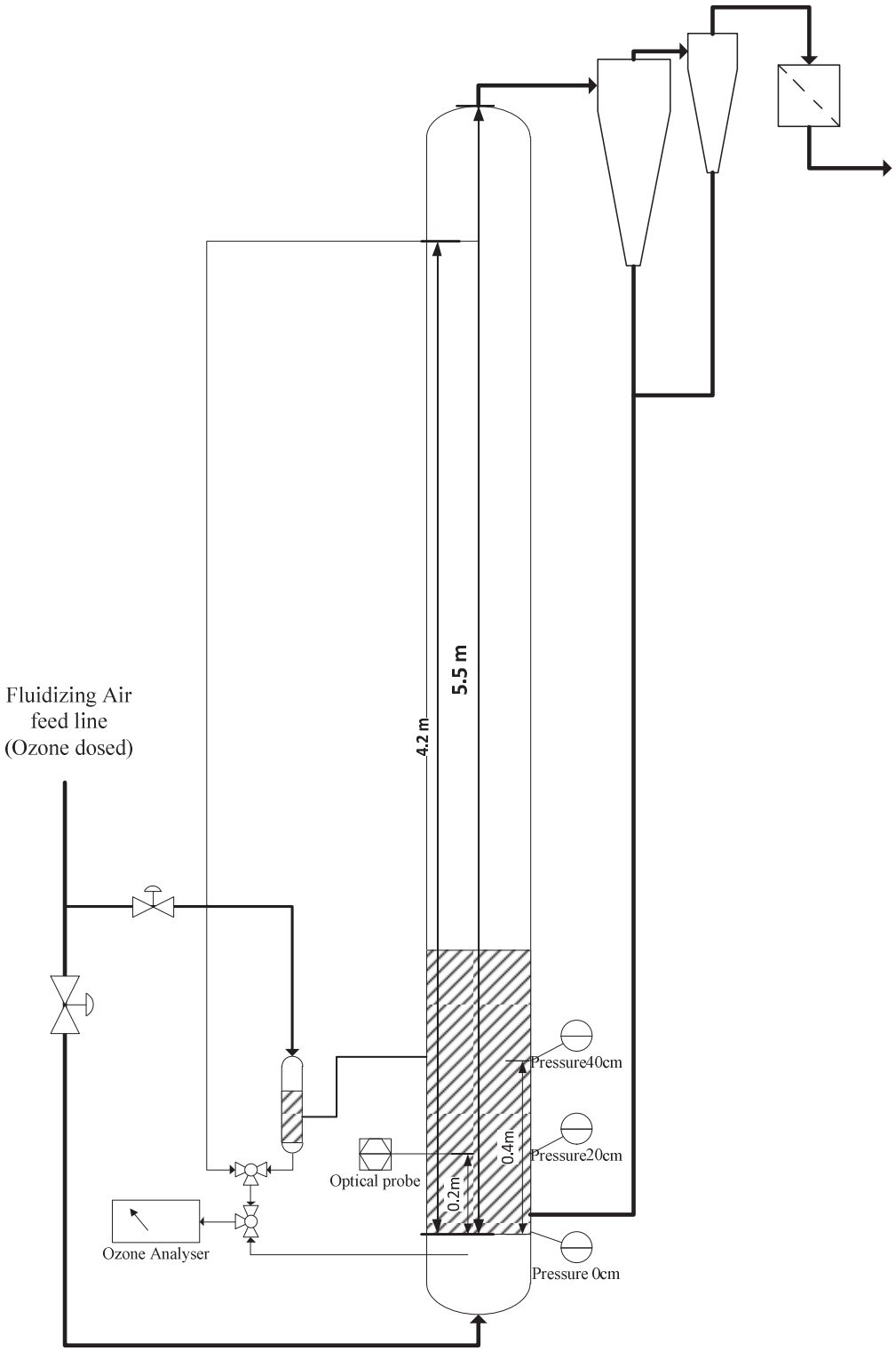
Fluidizing Air
feed line
(Ozone dosed)
5.5 m
4.2 m
Pressure40cm
Pressure20cm
Pressure 0cm
0.4m
0.2m
Optical probe
Ozone Analyser

Figure 1

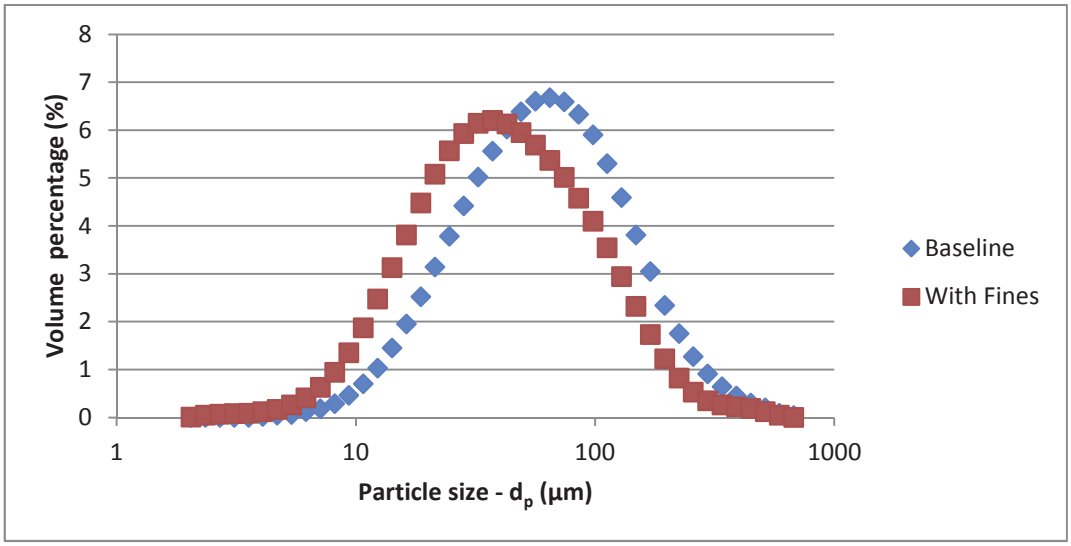
8
7
6
5
4
3
2
1
0
Volume percentage (%)
1
10
100
1000
Particle size - d_p (µm)
Baseline
With Fines

Figure 2

(a)

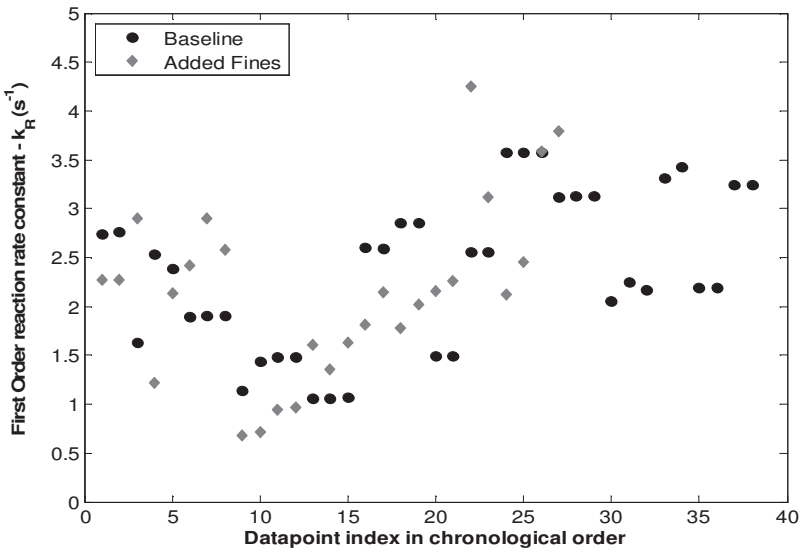
Baseline
Added Fines
First Order reaction rate constant - k_R (s^{-1})
Datapoint index in chronological order
0
0.5
1
1.5
2
2.5
3
3.5
4
4.5
5
0
5
10
15
20
25
30
35
40

(b)

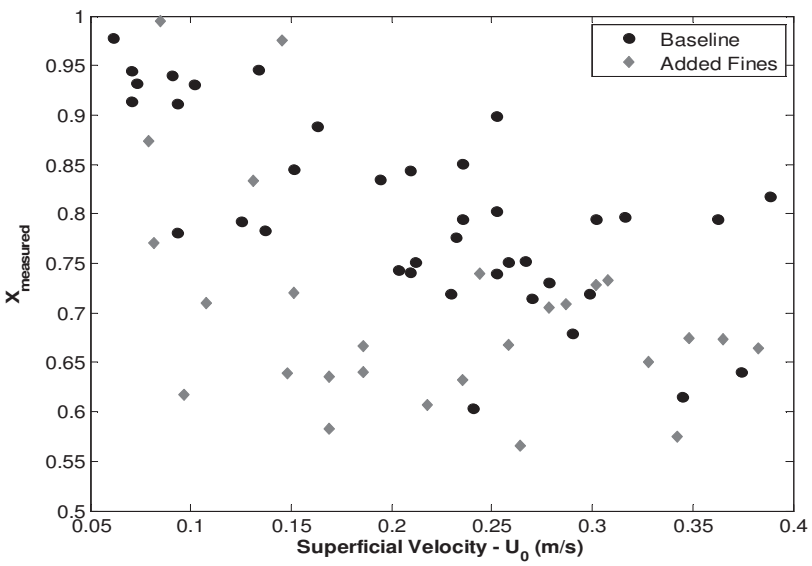
Baseline
Added Fines
$X_{measured}$
Superficial Velocity - U_0 (m/s)
0.5
0.55
0.6
0.65
0.7
0.75
0.8
0.85
0.9
0.95
1
0.05
0.1
0.15
0.2
0.25
0.3
0.35
0.4

Figure 3

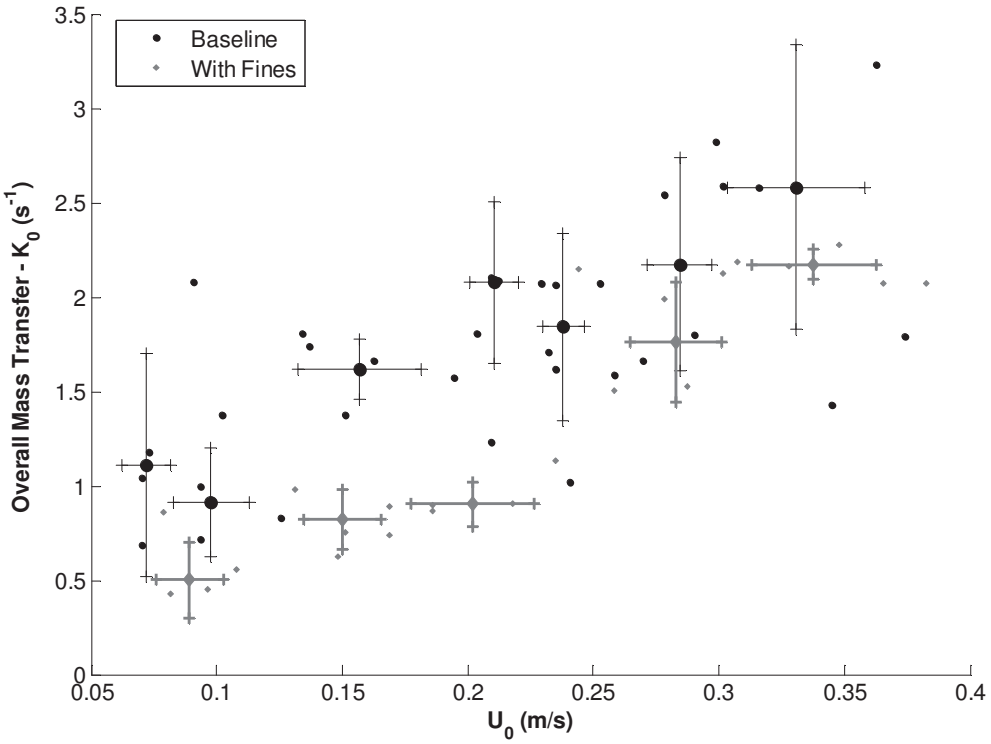
Baseline
With Fines
Overall Mass Transfer - K_0 (s^{-1})
U_0 (m/s)
0
0.5
1
1.5
2
2.5
3
3.5
0.05
0.1
0.15
0.2
0.25
0.3
0.35
0.4

Figure 4

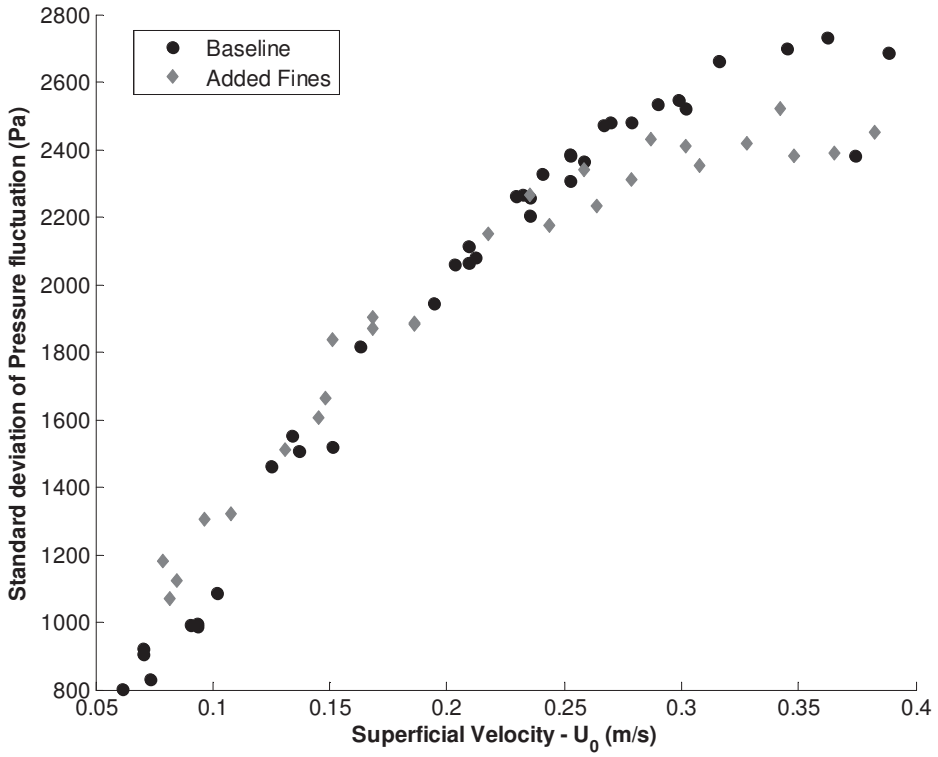
Baseline
Added Fines
Standard deviation of Pressure fluctuation (Pa)
Superficial Velocity - U0 (m/s)
2800
2600
2400
2200
2000
1800
1600
1400
1200
1000
800
0.05
0.1
0.15
0.2
0.25
0.3
0.35
0.4

Figure 5

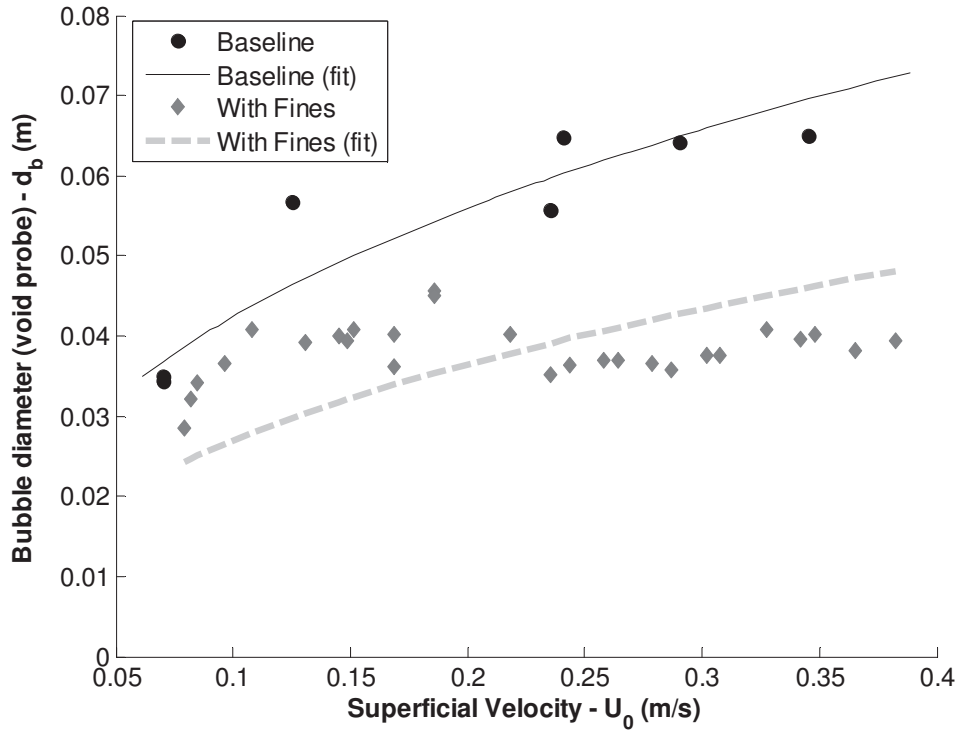
Baseline
Baseline (fit)
With Fines
With Fines (fit)
Bubble diameter (void probe) - d_b (m)
Superficial Velocity - U_0 (m/s)
0.08
0.07
0.06
0.05
0.04
0.03
0.02
0.01
0
0.05
0.1
0.15
0.2
0.25
0.3
0.35
0.4

Figure 6

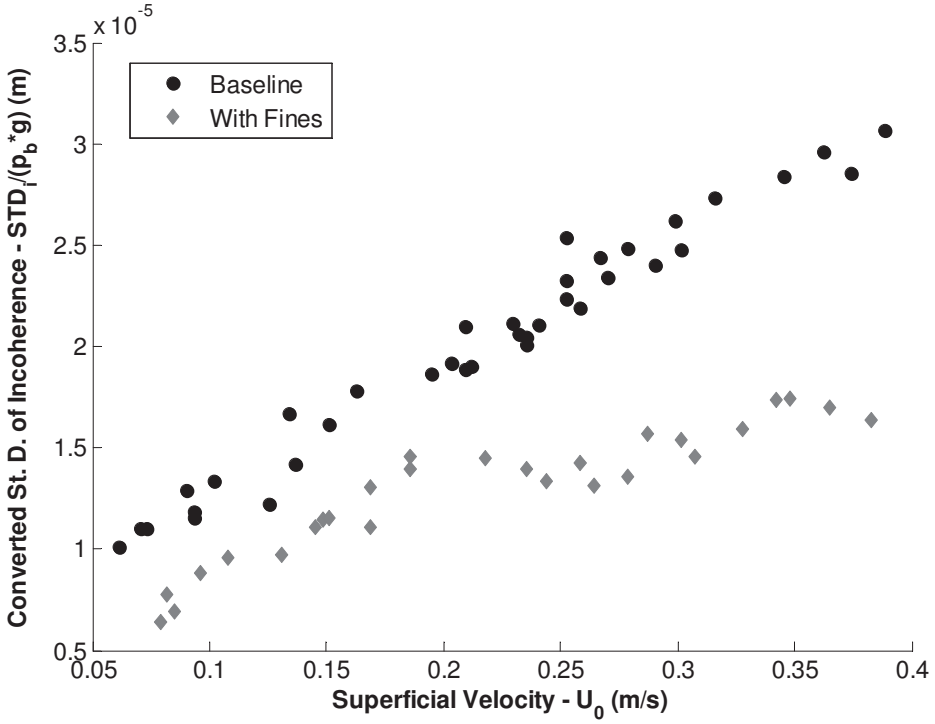
x 10^-5
3.5
3
2.5
2
1.5
1
0.5
Baseline
With Fines
Converted St. D. of Incoherence - STD_I/(p_b*g) (m)
0.05
0.1
0.15
0.2
0.25
0.3
0.35
0.4
Superficial Velocity - U_0 (m/s)

Figure 7

Figure 8

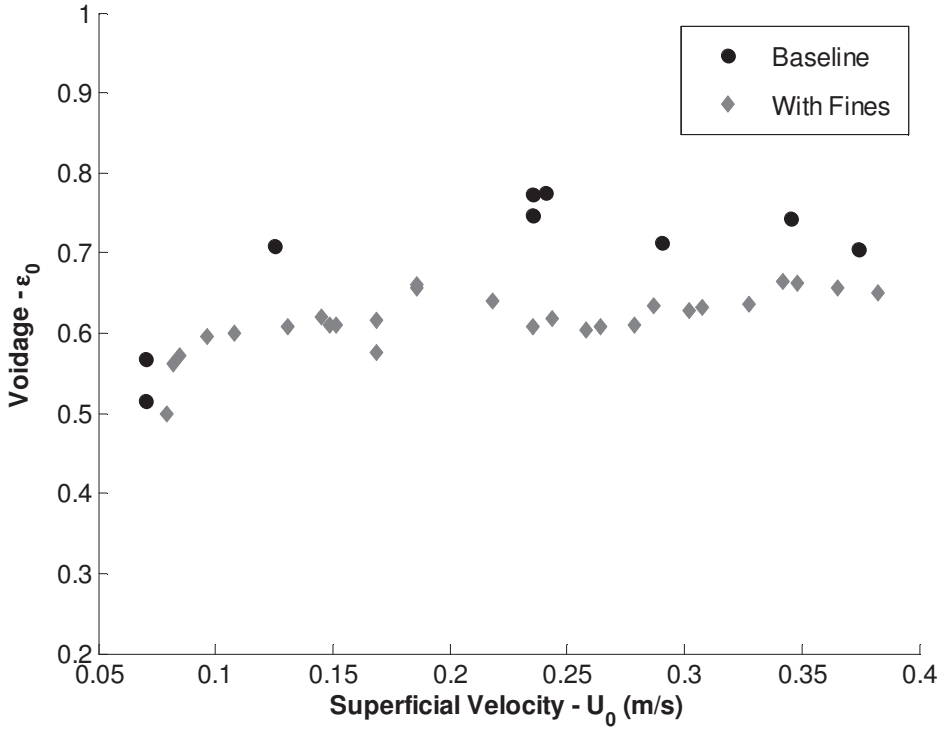

Figure 8

Figure 9

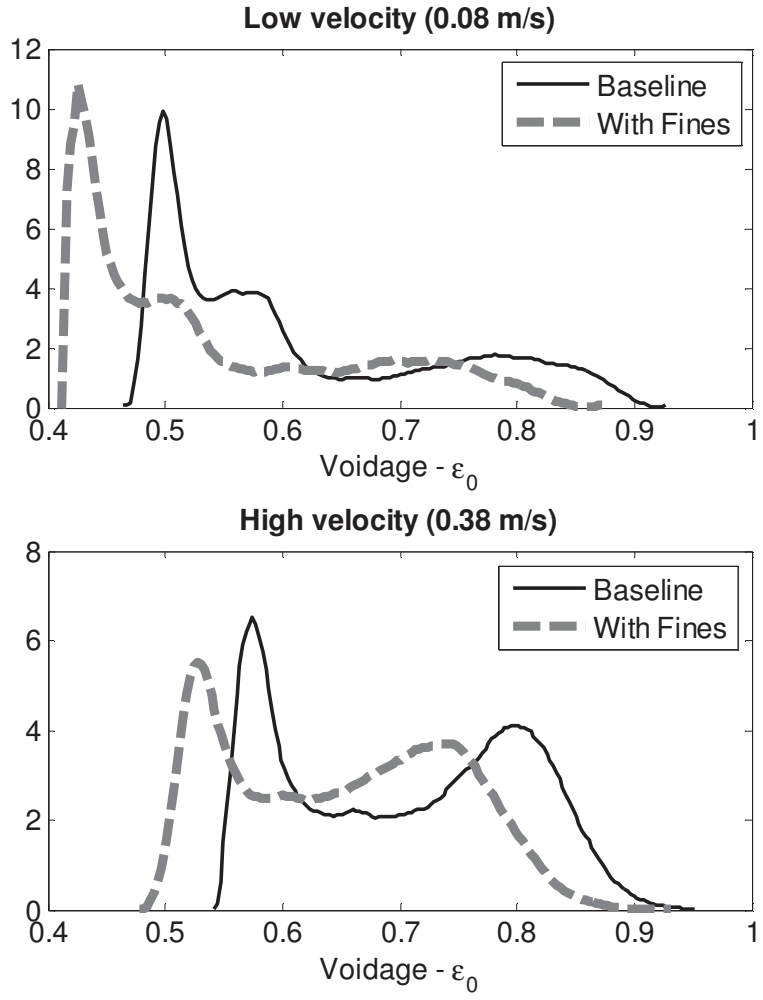

Figure 9

Figure 10

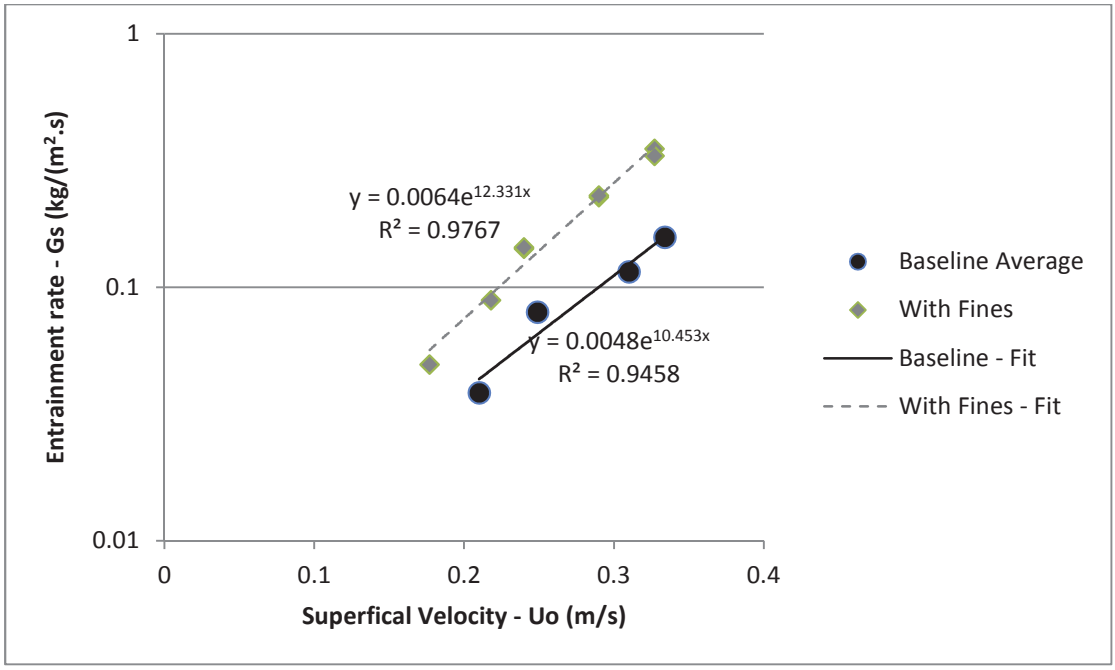

Figure 10

Figure 11

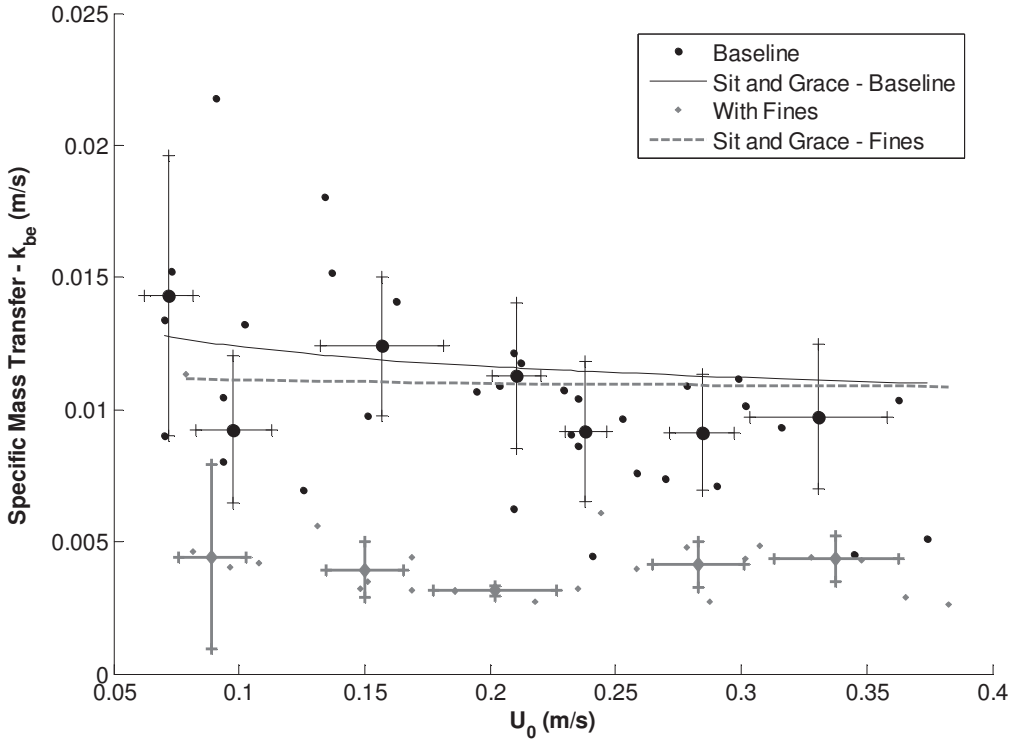

Figure 11

Table 1

Table 1

	FeSi (Baseline)	FeSi (With fines)
ρ_p (kg/m^3)	6,690	6,690
ρ_b (kg/m^3)	3,650	3,920
(μm)	59	41
Geldart	A/B	A/B
u_{mf} (mm/s)	6.5	5.0
ε_{mf}	0.46	0.42
μ_g (Pa.s)	18 x 10^{-6}	18 x 10^{-6}
ρ_g (kg/m^3)	1.2	1.2
D_m (m^2/s)	20 x 10^{-6}	20 x 10^{-6}

Highlights

- The effect of fines was investigated in a high-density particle fluidized bed.
- Reactor performance was quantified using an apparent mass transfer parameter.
- The addition of fines unexpectedly decreased the reactor performance, as well as the dense-phase voidage.
- The decrease in dense-phase voidage seems to counteract the effects of smaller bubbles.